High-Density Hydration Layer of Lysozymes: Molecular Dynamics Decomposition of Solution Scattering Data

Franci Merzel*,† and Jeremy C. Smith‡

National Institute of Chemistry, Hajdrihova 19, 1000 Ljubljana, Slovenia, and Computational Molecular Biophysics, IWR, University of Heidelberg, Im Neuenheimer Feld 368, D-69120 Heidelberg, Germany

Received May 18, 2005

A characterization of the physical properties of protein hydration water is critical for understanding protein structure and function. Recent small-angle X-ray and neutron scattering data indicate that the density of water on the surface of lysozyme is significantly higher than in bulk water. Here, we provide an interpretation of the scattering results using a molecular dynamics simulation, which allows us to make quantitative predictions about density variations in the first hydration shell. The perturbation relative to bulk water involves statistically significant changes in the average water structure in the first hydration layer. The water density in the first hydration shell is increased by 5% with respect to the bulk. In regions of higher water density, the water dipoles align more parallel to each other and the number of hydrogen bonds per water molecule is higher. Increased water density is found for water molecules interacting with hydrogen and carbon atoms in the backbone or with nonpolar or negatively charged side-chain groups.

1. INTRODUCTION

Water is recognized to have a critical role in influencing protein structure, folding, and function.[1,2] There has been renewed interest in protein hydration recently, due largely to new information on surface water that has been provided by X-ray crystallography, NMR spectroscopy, and computer simulation techniques. High-resolution X-ray and neutron diffraction methods are able to reveal water structure.[3,4] Also, NMR methods provide dynamic information such as the residence times of waters at certain locations.[5,6] However, the information that can be gained from any specific experimental technique is limited. For example, crystallographic and NMR information has been largely confined to relatively highly ordered internal and surface water molecules. Therefore, there is a need to directly characterize protein-induced solvent perturbation in terms of intrinsic properties of the system and that are independent of the experimental biases used to measure them. In this respect, molecular dynamics (MD)[7−10] simulation is particularly promising as it, in principle, provides complete information on the protein−water system.[11−13] However, MD is also subject to methodological errors, for example, in the force field and simulation protocol, and time scale limitations restrict the configurational sampling available. Therefore, it is essential to validate MD by direct comparison with experimental data, normally by using vibrational analysis,[14−16] before proceeding to decompose the trajectories, so as to provide detailed information on the intrinsic structures of interest.

To complement the methods that provide specific local information on a few strongly perturbed water molecules, there is a need to obtain a more global picture in which the average properties of water molecules on a protein surface are compared with those of the bulk. Small-angle scattering (SAS) techniques are well-suited for this and provide information on low- and medium-resolution average structural features of the examined system.[17]

In recent work, Svergun et al.[18] combined neutron and X-ray scattering to re-examine protein-induced solvent perturbation. The scattering profile results for lysozyme were interpreted with a model in which the protein atoms were included explicitly as the static X-ray crystallographic structure and the solvent as a continuum. When this model was used, it was shown that the average density of the first hydration shell of lysozyme (0−3 Å) is significantly higher than that of bulk water, and a value of ∼10% increased density was estimated.

In our previous work,[19,20] we derived SAS profiles for lysozyme in an explicit water environment using MD simulation. The simulation-derived scattering profiles were found to be in excellent agreement with experimental results. Further analysis revealed the net enhancement of water density in the first hydration shell as 5% over bulk water. Variation in the first hydration shell density was shown to be correlated with electrostatic properties of the protein surface and local surface topography.

Here, we use molecular dynamics simulations of lysozyme in explicit water to demonstrate the influence of the hydration layer density on the shape of the calculated SAS pattern. Subsequently, we provide a detailed analysis of structural properties of the hydration water such as radial distribution functions in the vicinity of different types of protein atoms, orientational properties of water, hydrogen bonding, and so forth.

2. METHODS

Using the MD program CHARMM,[21] we simulated the system of the hen-egg white lysozyme[22] in an explicit water

* Corresponding author. E-mail: franc@cmm.ki.si.
† National Institute of Chemistry.
‡ University of Heidelberg.

10.1021/ci0502000 CCC: $30.25
Published on Web 10/14/2005

environment consisting of approximately 30.000 atoms as described in detail elsewhere.[20] To summarize, a 2-ns-long trajectory of the system was generated under constant pressure and temperature. Periodic boundary conditions were applied, and the unit cell was chosen to be a truncated octahedron. The water was modeled using the TIP3P[23] potential.

Being able to trace each individual atom in the system throughout the simulation, we can evaluate the solution scattering intensity by orientational and configurational averaging of the square of the scattering amplitude $A(\mathbf{q}, t)$, given by

$$A(\mathbf{q}, t) = \sum_{j}^{N} [b_j - \bar{b}_0 V_j f_j(q)] \exp[-i\mathbf{q}\,\mathbf{r}_j(t)] \qquad (1)$$

Here, the subscript j runs over all atoms and b_j corresponds to the scattering length of an atom j, V_j is the atomic excluded volume, which is atom-type-specific, f_j is the corresponding form factor, and $\bar{b}_0$ is the scattering length density of the bulk. In evaluating the total scattering profile of the system, we achieve a significant computational speed-up by using the well-known angular plane-wave expansion, which gives rise to a multipole expansion of the scattering amplitude

$$A(\mathbf{q}, t) = \sum_{l=0}^{l_{\max}} \sum_{m=-l}^{l} A_{lm}(q, t)\, Y_{lm}(\Omega_{\mathbf{q}}), \qquad l_{\max} = 17 \quad (2)$$

with the multipole moments

$$A_{lm}(q, t) = 4\pi i^l \sum_{k}^{N} [b_k - \bar{b}_0 V_k f_k(q)] j_l[q r_k(t)] Y^*_{lm}[\omega_{\mathbf{r}_k}(t)] \qquad (3)$$

where j_l and Y_{lm} are the spherical Bessel functions and spherical harmonics, respectively. The resulting formula for the scattering intensity requires only the time average of the sum over the multipole moments of scattering amplitudes: For more details, see ref 20.

$$I(q) = \langle \sum_{lm} |A_{lm}(q, t)|^2 \rangle_t \qquad (4)$$

Now we would like to raise the question of to what extent the perturbation of the solvent, due to the presence of the protein, affects the SAS profiles. As it is known from previous work,[19] most structural changes of the solvating water concern the first hydration shell. An explicit way of determining the effect of surface water density variation on the scattering profiles is to uniformly modify the scattering lengths of the atoms within the first hydration shell by introducing the scaling factor λ

$$b_k = \begin{cases} \lambda b_k & \text{if atom } k \text{ is in first hydration layer} \\ b_k & \text{otherwise} \end{cases} \qquad (5)$$

Redefined scattering lengths b_k can be inserted into eq 3 and the scattering intensity rederived using eq 4 for each selected value of λ. Shape differences between individual scattering curves caused by the density variations in the first hydration shell can be well-summarized by differences between radii of gyration R_g. These can be derived from the slope of the scattering curves at very small q values using the Guinier formula [$I(q) \sim 1 - 1/3q^2R_g^2$].

If the solvent were unperturbed from the bulk because of the presence of protein, then the scattering profile derived from a model in which the solvent is treated as a uniform continuum would fully reproduce the experimental data. Furthermore, the variation of scattering lengths has the same effect as changing the particle density. If we now assume that the density in the first hydration shell is increased and that the explicit solvent MD model well reproduces this effect, then we should be able to find some scaling factor $\lambda < 1$, such that the radius of gyration from the explicit solvent model matches the radius of gyration derived from the uniform continuum solvent model. From the comparison of SAS results, we can, in turn, obtain a good approximate value of the overall density enhancement in the first hydration shell, which is equal to $1 - \lambda$.

The basic structural property studied in the hydration problems is the radial distribution function for water molecules around a given solute. The most straightforward way of deriving this is to slice the solvent space around the solute into radially concentric shells and count the number of water molecules that are found within the layers. The final radial distribution function is given as the average over the coordinate sets available in the trajectory of the system. Even if the protein surface appears to be rather complicated, it turns out it has an approximate globular shape if the protein is in its native state. This allows us to derive a good approximation to define the protein surface S_P in terms of spherical coordinates $\omega = (\theta, \phi)$ in a multipole expansion

$$S_P(\omega) = \sum_{l=0}^{L_{\max}} \sum_{m=-l}^{l} \mathscr{R}_{lm} \mathscr{Y}_{lm}(\omega) \qquad (6)$$

The origin of the coordinate system is the protein center of mass. $\mathscr{Y}_{lm}$ is the real spherical harmonic function, and $\mathscr{R}_{lm}$ is the corresponding expansion coefficient, which is given by numerical angular integration on the so-called Lebedev grid[24]

$$\mathscr{R}_{lm} = \int_0^{2\pi} \mathrm{d}\phi \int_0^{\pi} \sin(\theta)\, S_P(\omega)\, \mathscr{Y}_{lm}(\omega)\, \mathrm{d}\theta = \sum_{k}^{N_P} w_k r_k \mathscr{Y}_{lm}(\omega_k) \quad (7)$$

Here, the subscript k runs over the N_P grid points, w_k is the integrating weight for the spatial angle ω_k, and r_k is the radial intersection point between the space occupied by the protein and that occupied by the solvent. The advantage of a surface thus defined is its analytical form, which can significantly contribute to the simplicity of the subsequent analysis.

We define a closed layer at distance d from the protein surface with a radial thickness δ in terms of spherical coordinates as space between upper $S_P(\omega) + d + \delta/2$ and lower $S_P(\omega) + d - \delta/2$ boundaries with respect to the center of mass of the protein. The number of water molecules that reside within this layer is $N_w(d, \delta)$. The average number density of water molecules at a distance d from the protein surface S_P is then

$$\bar{\rho}(d) = \left\langle \frac{N_w(d, \delta)}{V(d, \delta)} \right\rangle_t \qquad (8)$$

where $\langle X \rangle_t$ denotes a time average and $V(d, \delta)$ is the volume of the layer, given by

$$V(d, \delta) = \frac{1}{3}\sum_{k}^{N_P} w_k\{[S_P(\omega_k) + d + \delta/2]^3 - [S_P(\omega_k) + d - \delta/2]^3\} \quad (9)$$

For the integration (summation) in eq 9, the same mesh points are used as for the calculation of the protein surface. The average number density, eq 8, in any given layer is obtained by averaging over the simulation trajectory. For each of the 2000 saved structures of the protein generated by the MD trajectory, the corresponding protein surface was determined and the number of water molecules in each layer counted.

In addition to dividing the space around the protein into concentric layers, angular partitioning can also be introduced. In this way, the solvent properties on selected localized regions of the protein surface can be analyzed. In principle, it should suffice to weight the selected region on the layer by 1 and the remaining surface by 0. However, since any discontinuity is difficult to represent with smooth functions, the spherical harmonic representation of angular step functions has poor convergence. Therefore, it is meaningful to introduce weighting functions as narrow "bumps", that is, angular Gaussian functions g_{ki}, of maximum value 1 at directional angle ω_k on the spherical surface. The width of the angular Gaussian function is determined by the average angle between two neighboring mesh points on the spherical surface. We define a set of weights on the entire grid consisting of directional angles i for each selected direction k

$$g_{ki} = \exp\left[-\left(\frac{\varphi_{ki}}{\varphi_0}\right)^2\right],$$
$$\varphi_{ki} = \arccos[\sin(\theta_k)\sin(\theta_i)\cos(\phi_k - \phi_i) + \cos(\theta_k)\cos(\theta_i)] \quad (10)$$

where $\varphi_0 = 2/\sqrt{N_P}$ is the average angle between two neighboring grid points from the Lebedev integration scheme.

3. RESULTS

First, we demonstrate the agreement between the calculated solution X-ray SAS for lysozyme from simulation and experimental data, see Figure 1A. While the agreement is found to be excellent for the explicit solvent model (in which density variations of the solvent are present), it fails for the uniform continuum solvent model with bulk solvent density. In a second set of calculations, the water molecules around the protein that are up to 4 Å apart from the protein atoms were selected; the first hydration layer is, thus, assumed to be 3-Å-thick, and 1 Å corresponds to half the thickness of the interfacial region between the protein and solvent. The scattering length scaling factors assigned to the atoms in the first hydration shell were varied, and corresponding profiles for $\lambda = \{0.9, 1.0, 1.1\}$ are shown in Figure 1B. Using the Guinier formula,[17] we derived radii of gyration, R_g, from the slope of the scattering curves. The dependence of R_g on λ is shown in Figure 1C. Knowing the correct radius of gyration, R_g^{es}, from the explicit solvent model and the one from the uniform continuum solvent model, R_g^{ucs}, the corresponding difference on the abscissa, $\lambda_{es} - \lambda_{ucs} = 1 - \lambda_{ucs}$, can be found. This value is found to be ~0.05. This means that the scattering lengths of the atoms in the first hydration shell must be reduced by 5% in order to compensate for the density variation present in the explicit-atom simulation. We can conclude, in turn, that the solvent density is increased by 5%.

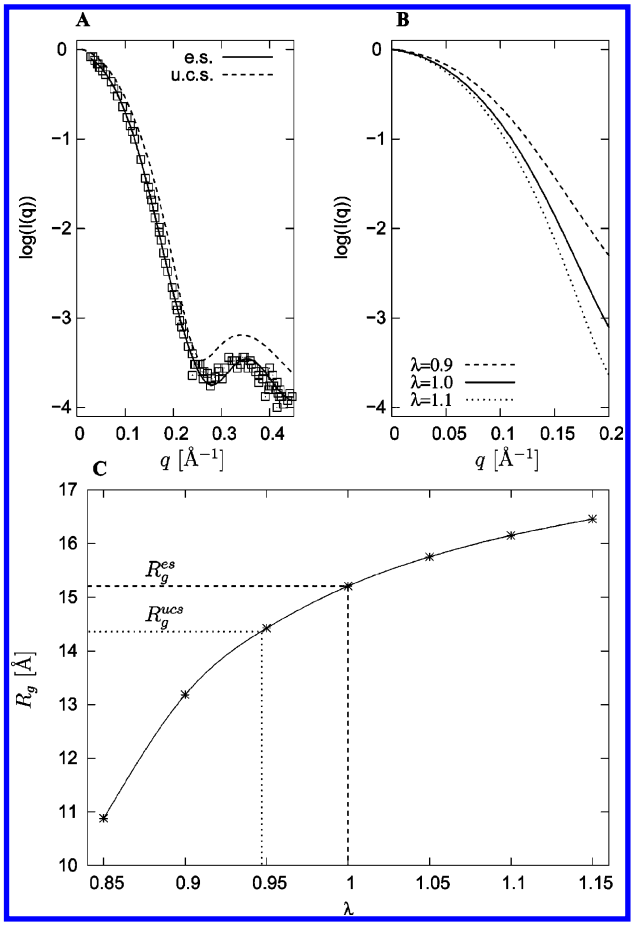

Figure 1. (A) Experimental X-ray scattering (squares) compared with calculated scattering from the explicit solvent model (solid line, es) and the uniform continuum solvent model (dashed line, ucs). (B) Scattering curves at different values of the scattering length scaling factor $\lambda = \{0.9, 1.0, 1.1\}$ introduced in the first hydration shell, eq 5. (C) Derived radii of gyration from the explicit solvent model (solid line) as a function of the scattering length scaling factor introduced in the first hydration shell. R_g^{es} corresponds to the radius of gyration due to the explicit solvent model with $\lambda = 1$. R_g^{ucs} is the radius of gyration derived from the uniform continuum solvent model.

To calculate the radial distribution functions of water around the protein, the protein surface was obtained using the multipole expansion of eq 6 with the resolution $L_{max} = 29$. The Lebedev grid consisted of $N_P = 1202$ grid points. The solvent space was divided into $\delta = 1$-Å-thick concentric layers from $d = 0-6$ Å out from the protein surface. The layers were chosen to be located equidistantly at a separation of 0.2 Å so as to produce a smooth density profile. The calculated protein surface corresponds to the value $d = 0$. The average number density, eq 8, in any given layer is obtained by averaging over the simulated trajectory. For each of the 2000 saved frames of the system trajectory, the corresponding protein surface was determined as well as the number of water molecules in each layer. We calculate the

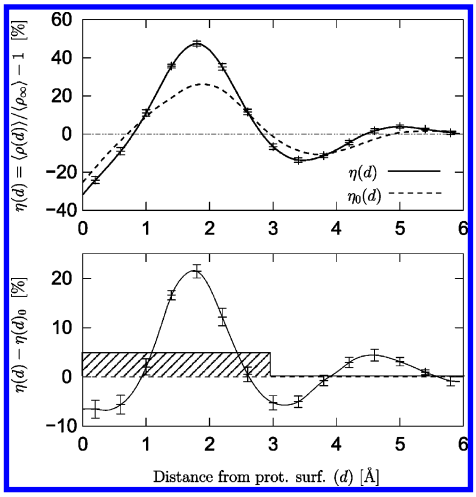

Figure 2. Radial water density profile around the protein and perturbation from the bulk density profile due to the protein−solvent interaction as a function of the distance from the protein surface. Error bars denote the statistical error due to dynamical fluctuations appearing during the simulation.

radial distribution function as the relative deviation of the average number density $\langle\rho(d)\rangle$, which is a function of the distance d from the protein surface, from the bulk density $\langle\rho_\infty\rangle$

$$\eta(d) = \left[\frac{\langle\rho(d)\rangle}{\langle\rho_\infty\rangle} - 1\right] \tag{11}$$

The density profile $\eta(d)$ of the water around the protein is shown in Figure 2. A significant high-density peak is seen, corresponding to the first hydration layer. In this peak, the water density is locally ∼40% higher than that of bulk water.

We now investigate to what extent the deviation of $\eta(d)$ from the average bulk value is due to perturbation of the water structure from that of bulk water. It is expected that there is a pure "geometric" or "correlation" effect in the distribution of atoms that would be present in the shell even if the water structure were unperturbed from the bulk. This effect should lead to a nonuniform density distribution. This is due to the fact that the surface is defined to pass between the two sets of atoms and, therefore, will be at a nonrandom distance from the water oxygens. Therefore, the structure of the bulk water radial distribution function is expected to be at least partly reflected in $\eta(d)$. To determine this "unperturbed water" contribution, the protein surface was superimposed onto the pure bulk water simulation system and the water molecules inside the surface were denoted as a fictitious "protein" atoms. The procedure of deriving the surface was then repeated for the fictitious protein and the corresponding water density profile, $\eta_0(d)$, calculated. $\eta_0(d)$, therefore, corresponds to what would be expected if the water around a protein were structurally unperturbed from the bulk behavior. The results are shown as the dashed line on the upper plot of Figure 2. Indeed, $\eta_0(d)$ resembles $\eta(d)$. The lower plot shows $\eta(d) - \eta_0(d)$ and, thus, gives the perturbing effect of the protein on the radial density distribution. Integration of this over $d = 0-3$ Å gives ∼5%, which is exactly the same as the value obtained in the SAS analysis.

The results presented so far have concerned average properties of the hydration water and their influence on

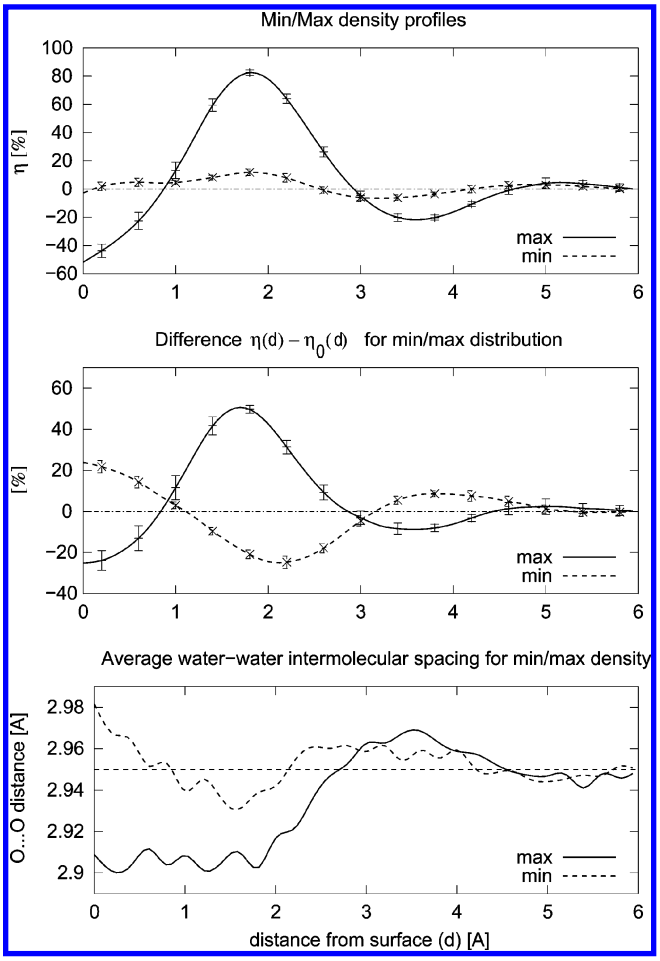

Figure 3. Radial density profiles for the surface sections with 10% highest and 10% lowest local densities and corresponding average water O···O distance distributions.

scattering profiles. In what follows, we use the simulation to decompose the observed density effects and to examine heterogeneity in the surface hydration. We need to introduce angular partition, using eq 10, for dividing radial shells into smaller sections. Density profiles associated with regions of the ∼10% highest and lowest densities are shown in Figure 3. The difference between two cases is large, indicating that the radial density profiles exhibit considerable heterogeneity. The contraction of the average O···O distance (lower plot of Figure 3) correlates well with the increase/decrease of the density.

To further describe the density variations, slices of density, $\eta(d, \omega)$, averaged in the shells of $d = 1.0-1.5$, $1.5-2.0$, and $2.0-2.5$ Å, were projected onto a sphere. The shells were chosen so as to represent the spatial density distribution around the first density peak. The corresponding polar plots for the upper and lower hemispheres are shown in Figure 4. A high degree of heterogeneity in the surface distribution of the density is revealed.

The heterogeneity of the density indicates that it is appropriate to investigate further how the density and associated structural properties vary at chemically different sites on the surface. To do this, we analyzed the dependence of water structural properties on the surface atom type. The protein atoms were divided into 13 types, according to their common chemical nature. Four hydrogen atom types were defined (hydrogen atoms in positively charged polar groups,

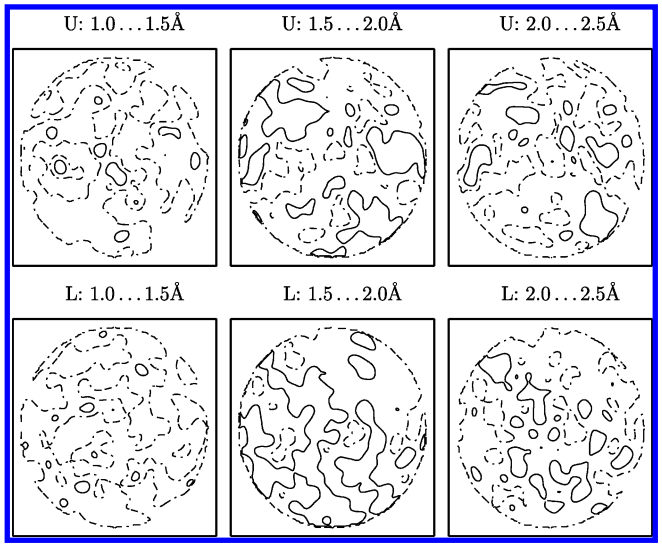

Figure 4. Polar plots showing the heterogeneity in the averaged water density in three layers above the protein surface projected onto a spherical surface. Letter "U" refers to the results on the "upper" hemisphere and letter "L" to the lower. Contours correspond to 25% (dot−dashed lines) and 50% (solid lines) values of the local density distribution $\eta(d,\omega)$.

neutral polar groups, nonpolar groups, and the backbone), as were three oxygen types (in negatively charged groups, polar groups, and the backbone), three nitrogen types (in positively charged groups, polar groups, and the backbone), and three carbon types (in neutral polar and nonpolar groups and the backbone).

The five protein surface atoms closest to each Lebedev grid point on the protein surface were selected. On average, these atoms are enclosed in a sphere of 3 Å radius around the grid point. The chemical character of the grid point was defined as a weighted average of the contributing atom types. In this way, changes in the solvent density can be analyzed in terms of the chemical nature of the protein surface.

Figure 5 shows the density profiles $\eta(d, \omega)$ associated with the different atomic types. The overall form of the profiles due to different types of atoms is quite similar and does not explain the whole range of density variations shown on the min/max density profile in Figure 3. Detailed information on the decomposition of the density profiles according to the chemical type is collected in Table 1.

A large perturbation effect is due to water molecules associated with the negatively charged oxygens, for which the distribution is shifted to small distances. Furthermore, the backbone and nonpolar atoms also have a large perturbative effect, with a more pronounced first maximum and higher root-mean-square deviation from the bulk water profile than those for the polar atoms and even more so than those for the positively charged atoms. Given the relatively large fraction of the protein surface made up by the nonpolar and backbone hydrogens and carbons (60%), these are expected to produce the largest perturbative effect on the average density.

It is of interest to examine whether there is some correlation between the density variations and water molecule dipole orientations, that is, the mutual orientation of neighboring water molecules. This information can be obtained from analyzing the orientational distribution w_ϕ of dipoles from neighboring water molecules. The upper plot of Figure

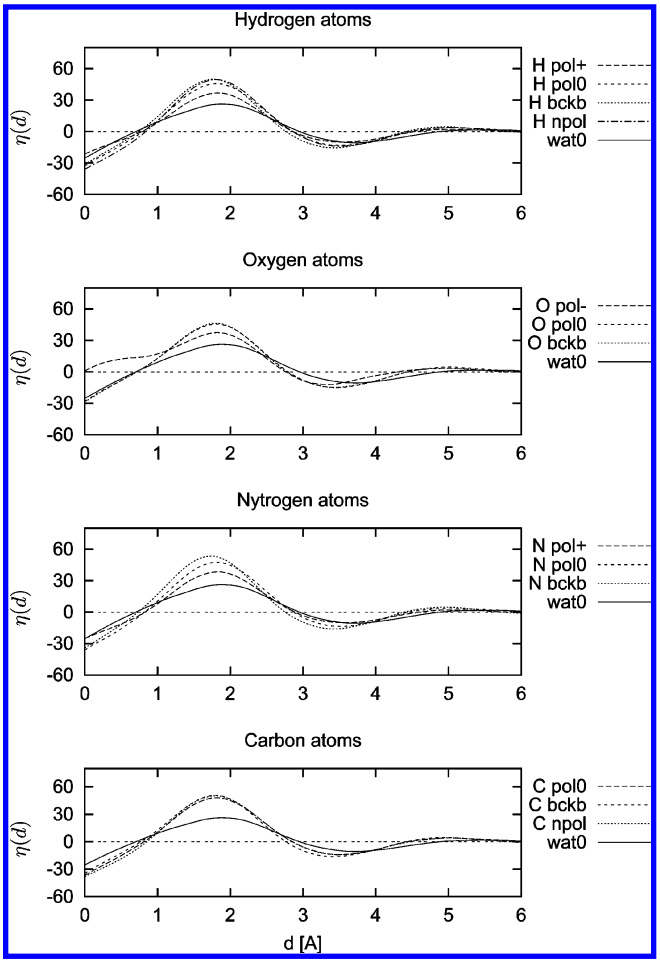

Figure 5. Density profiles $\eta(d,\omega)$ in the vicinity of different types of atoms on the protein surface. "pol" indicates that the given atom forms part of polar group. "+", "0", and "−" denote net charges on the associated group. "bckb" and "nplr" denote atoms belonging to the protein backbone and nonpolar/hydrophobic groups, respectively, "wat0" denotes the unperturbed density distribution in the bulk.

6 shows the average orientational distribution of neighboring dipoles in an MD simulation of bulk water. This exhibits a characteristic form that originates mainly from the hydrogen-bonding interactions between neighboring water molecules. This distribution tells us that the most probable alignment of two neighboring dipoles in bulk water is parallel. The middle plot of Figure 6 shows the perturbation of the water dipole orientations with respect to the average distribution in the bulk in two different layers. As the protein surface is approached, the tendency to populate lower angles becomes more pronounced. The lower plot shows the $d = 1-2$ Å perturbation in those regions on the protein surface corresponding to the highest and lowest 10 local densities. Clearly, with increasing density, the dipoles align more parallel to each other.

As a consequence of the above results, one might expect more intensive hydrogen bonding in the case of higher water density. In Figure 7 is presented the number of water−water hydrogen bonds as a function of distance from the protein surface. The small number of hydrogen bonds at small distances is a direct consequence of the fact that water−protein interactions are not included. The plateau at $d \sim 3$ Å accompanies the transition into the second hydration layer, confirming the choice of $d = 0-3$ Å as the first hydration

Table 1. Characteristics of the Atom-Type-Dependent Water Density Profiles and Their Perturbation Due to the Protein−Solvent Interaction[a]

atom type	p[%]	$\overline{\eta(d)}_{(0-3)}$	$\overline{\eta(d) - \eta_0(d)}_{(0-3)}$	χ
H pol+	6.7	12.2 ± 1.0	2.6 ± 1.0	4.5 ± 1.4
H pol0	7.7	14.5 ± 0.9	4.9 ± 0.9	7.9 ± 0.8
H bckb	10.8	15.7 ± 0.5	6.1 ± 0.5	9.4 ± 0.4
H nplr	28.8	14.8 ± 0.5	5.1 ± 0.5	9.6 ± 0.6
O pol-	3.1	17.7 ± 1.1	8.0 ± 1.1	10.2 ± 1.1
O pol0	5.5	15.2 ± 1.0	5.5 ± 1.0	7.8 ± 0.6
O bckb	3.4	15.1 ± 1.1	5.5 ± 1.1	8.1 ± 0.9
N pol+	3.0	12.2 ± 1.1	2.5 ± 1.1	5.0 ± 1.3
N pol0	3.4	14.6 ± 1.0	4.9 ± 1.0	9.0 ± 0.9
N bckb	2.1	16.8 ± 0.9	7.2 ± 0.9	11.0 ± 0.8
C pol0	2.5	14.6 ± 1.2	5.0 ± 1.2	9.2 ± 1.2
C bckb	7.5	15.3 ± 0.6	5.7 ± 0.6	9.8 ± 0.6
C nplr	13.2	14.4 ± 0.4	4.7 ± 0.4	10.1 ± 0.8
average	100.0	14.8 ± 0.4	5.1 ± 0.4	8.3 ± 0.5

[a] In the first column are specified protein atomic types on the protein surface. In the second column, the fraction of the surface occupied by the given atomic type is given. Average densities within the first layer of thickness 3 Å are given in the 3rd and 4th columns. In the last column the root-mean-square deviation, χ, defined as $\chi^2 = 1/D \int_0^D [\eta(x) - \eta_0(x)]^2 \, dx$, where $D = 6$ Å, is given—this quantity quantifies the overall perturbation of the density profile due to the protein−solvent interaction. The last row gives the column averages.

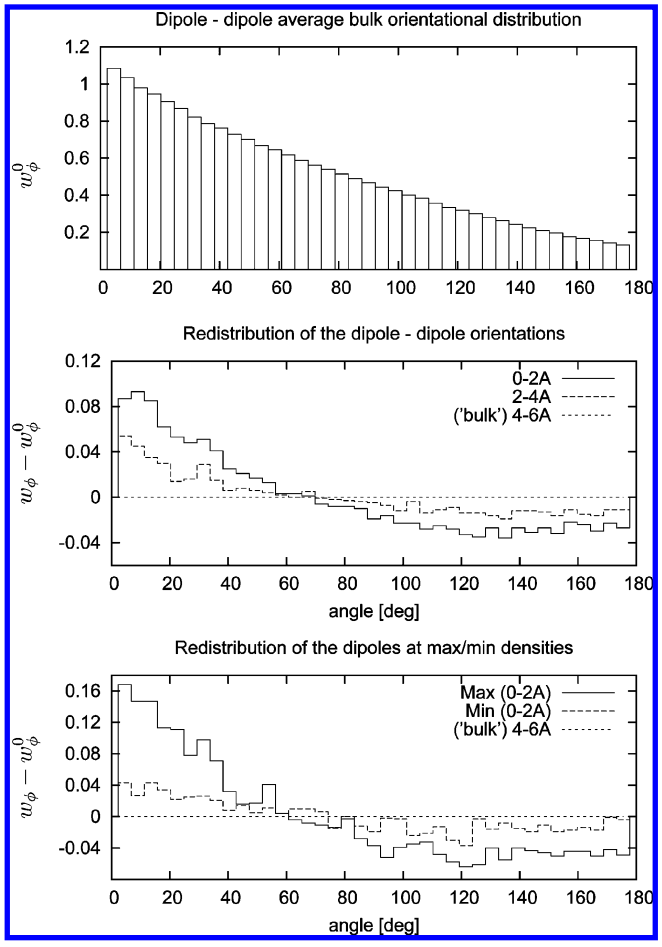

Figure 6. Mutual orientation w_ϕ of neighboring water dipoles.

layer. According to the geometric hydrogen-bond criteria used here,[25] the average number of hydrogen bonds formed by an individual water molecule in the bulk is 3.4. The lower plot shows the difference in the frequency of forming hydrogen bonds for the regions of maximum and minimum densities. Hydrogen bonding is significantly more frequent in the regions with higher density, in harmony with the dipole distribution results.

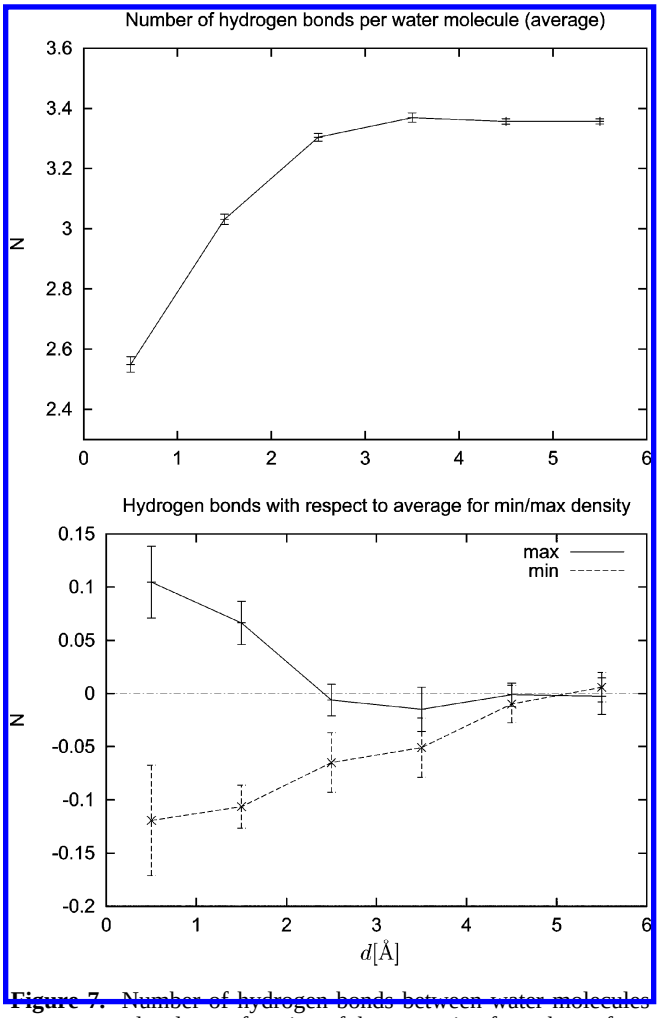

Figure 7. Number of hydrogen bonds between water molecules per water molecule as a function of the separation from the surface. Also shown are the cases corresponding to maximal and minimal densities. Only hydrogen bonds between water molecules are counted. Criteria for the determination of hydrogen bonds are based on geometric conditions.[25]

4. CONCLUSIONS

The present work examines structural characteristics of water in the hydration layer around a protein. The dynamically averaged solvent structure was obtained through the time average over a molecular dynamics trajectory. The computational framework used in this work allows a fast analysis of the water structure in hydration layers of arbitrary globular proteins, providing efficient insight into protein hydration. Comparisons between experimental and simulated X-ray solution SAS provided quantitative predictions about density variations of the first hydration shell, which are studied here in detail. Water density in the first hydration shell is found to be increased by 5% with respect to the bulk because of protein−solvent interactions. The present work follows from previous results in which correlations between density variations and topographical and electrostatic properties of the protein surface were revealed.[19] This work provides further evidence about the structural changes of the protein surface water. In particular, a tendency is found of the water dipoles to align more parallel to each other as the

water density increases. The hydrogen-bond number density is also significantly increased in the regions with higher density. There is also a correlation between the density increase and the presence of oxygens on the negatively charged surface groups, backbone atoms, and nonpolar sites. However, no particular hydration pattern was found that significantly discerns between chemical properties of the protein surface (hydrophobic/hydrophilic, etc.). Water density enhancement in the vicinity of the backbone atoms is in full agreement with the correlation found for the surface topography and density/packing.[19,26] Backbone atoms are topographically more frequently located in surface grooves and cavities, which were shown to be of higher surface water density. A further understanding of the global hydration properties of proteins will require still more analysis of the various forces competing to determine surface water structure and dynamics.

REFERENCES AND NOTES

(1) Pettitt, B. M.; Makarov, V. A.; Andrews, B. K. Protein hydration density: theory, simulations and crystallography. *Curr. Opin. Struct. Biol.* **1998**, *8*, 218−221.

(2) Teeter, M. M. Water−protein interactions − theory and experiment. *Annu. Rev. Biophys. Biophys. Chem.* **1991**, *20*, 577−600.

(3) Carugo, O.; Bordo, D. How many water molecules can be detected by protein crystallography? *Acta Crystallogr., Sect. D* **1999**, *55*, 479−483.

(4) Schoenborn, B. P.; Garcia, A.; Knott, R. Hydration in protein crystallography. *Prog. Biophys. Mol. Biol.* **1995**, *64*, 105−119.

(5) Denisov, V. P.; Halle, B. Protein hydration dynamics in aqueous solution. *Faraday Discuss.* **1996**, *103*, 227−244.

(6) Wiesner, S.; Kurian, E.; Prendergast, F. G.; Halle, B. Water molecules in the binding cavity of intestinal fatty acid binding protein: Dynamic characterization by water O-17 and H-2 magnetic relaxation dispersion. *J. Mol. Biol.* **1999**, *286*, 233−246.

(7) Leach, A. R.; *Molecular Modelling: Principles and Applications*; Addison-Wesley Longman: Essex, England, 1996.

(8) Janežič, D.; Praprotnik, M.; Merzel, F. Molecular dynamics integration and molecular vibrational theory. I. New symplectic integrators. *J. Chem. Phys.* **2005**, *122*, 174101 (article number).

(9) Praprotnik, M.; Janežič, D. Molecular dynamics integration and molecular vibrational theory. II. Simulation of nonlinear molecules. *J. Chem. Phys.* **2005**, *122*, 174102 (article number).

(10) Praprotnik, M.; Janežič, D. Molecular dynamics integration and molecular vibrational theory. III. The infrared spectrum of water. *J. Chem. Phys.* **2005**, *122*, 174103 (article number).

(11) Abseher, R.; Schreiber, H.; Steinhauser, O. The influence of a protein on water dynamics in its vicinity investigated by molecular dynamics simulation *Proteins* **1996**, *25*, 366−378.

(12) Makarov, V. A.; Andrews, B. K.; Smith, P. E.; Pettitt, B. M. Residence times of water molecules in the hydration sites of myoglobin *Biophys. J.* **2000**, *79*, 2966−2974.

(13) Luise, A.; Falconi, M.; Desideri, A. Molecular dynamics simulation of solvated azurin: Correlation between surface solvent accessibility and water residence times *Proteins* **2000**, *39*, 56−67.

(14) Brooks, B. R.; Janežič, D.; Karplus, M. Harmonic-analysis of large systems. 1. Methodology. *J. Comput. Chem.* **1995**, *16*, 1522−1542.

(15) Janežič, D.; Brooks, B. R. Harmonic-analysis of large systems. 2. Comparison of different protein models. *J. Comput. Chem.* **1995**, *16*, 1543−1553.

(16) Janežič, D.; Venable, R. M.; Brooks, B. R. Harmonic-analysis of large systems. 3. Comparison with molecular-dynamics. *J. Comput. Chem.* **1995**, *16*, 1554−1566.

(17) Higgins, J. S.; Benoit, H. C. *Polymers and Neutron Scattering*; Calendron Press: Oxford, U. K., 1994.

(18) Svergun, D.; Richard, S.; Koch, M. H.; Sayers, Z.; Kuprin, S.; Zaccai, G. Protein hydration in solution: Experimental observation by X-ray and neutron scattering. *Proc. Natl. Acad. Sci. U.S.A.* **1998**, *95*, 2267−2272.

(19) Merzel, F.; Smith, J. C. Is the first hydration shell of lysozyme of higher density than bulk water? *Proc. Natl. Acad. Sci. U.S.A.* **2002**, *99*, 5378−5383.

(20) Merzel, F.; Smith, J. C. SASSIM: a method for calculating small-angle X-ray and neutron scattering and the associated molecular envelope from explicit-atom models of solvated proteins. *Acta Crystallogr., Sect. D* **2002**, *58*, 242−249.

(21) Brooks, B. R.; Bruccoleri, R. E.; Olafson, B. D.; States, D. J.; Swaminathan, S.; Karplus, M. CHARMM − a program for macromolecular energy, minimization, and dynamics calculations. *J. Comput. Chem.* **1983**, *4*, 187−217.

(22) Vaney, M. C.; Maignan, S.; RiesKautt, M.; Ducruix, A. High-resolution structure (1.33 angstrom) of a HEW lysozyme tetragonal crystal grown in the APCF apparatus. Data and structural comparison with a crystal grown under microgravity from SpaceHab-01 mission. *Acta Crystallogr., Sect. D* **1996**, *52*, 505−517.

(23) Jorgensen, W. L.; Chandrasekhar, J.; Madura, J. D.; Impey, R. W.; Klein, M. L. Comparison of simple potential functions for simulating liquid water. *J. Chem. Phys.* **1983**, *79*, 926−935.

(24) Lebedev, V. I. The 59th order of algebraic accuracy quadrature formula for sphere. *Dokl. Akad. Nauk* **1994**, *338*, 454−456.

(25) Luzar, A.; Chandler, D. Structure and hydrogen-bond dynamics of water-dimethyl sulfoxide mixtures by computer simulations. *J. Chem. Phys.* **1993**, *98*, 8160−8173.

(26) Gerstein, M.; Chothia, C. Packing at the protein-water interface. *Proc. Natl. Acad. Sci. U.S.A.* **1996**, *93*, 10167−10172.

CI0502000